


## Article

# Biofilm Formation in *Xanthomonas arboricola* pv. *pruni*: Structure and Development

Pilar Sabuquillo \* and Jaime Cubero \* 

Instituto Nacional de Investigación y Tecnología Agraria y Alimentaria (INIA), Ctra. de La Coruña km 7.5, 28040 Madrid, Spain

\* Correspondence: mpesc@inia.es (P.S.); cubero@inia.es (J.C.); Tel.: +34-913476863 (P.S.); +34-913474162 (J.C.)

**Abstract:** *Xanthomonas arboricola* pv. *pruni* (Xap) causes bacterial spot of stone fruit and almond, an important plant disease with a high economic impact. Biofilm formation is one of the mechanisms that microbial communities use to adapt to environmental changes and to survive and colonize plants. Herein, biofilm formation by Xap was analyzed on abiotic and biotic surfaces using different microscopy techniques which allowed characterization of the different biofilm stages compared to the planktonic condition. All Xap strains assayed were able to form real biofilms creating organized structures comprised by viable cells. Xap in biofilms differentiated from free-living bacteria forming complex matrix-encased multicellular structures which become surrounded by a network of extracellular polymeric substances (EPS). Moreover, nutrient content of the environment and bacterial growth have been shown as key factors for biofilm formation and its development. Besides, this is the first work where different cell structures involved in bacterial attachment and aggregation have been identified during Xap biofilm progression. Our findings provide insights regarding different aspects of the biofilm formation of Xap which improve our understanding of the bacterial infection process occurred in *Prunus* spp and that may help in future disease control approaches.

**Keywords:** *Xanthomonas*; bacterial aggregation; planktonic; *Prunus* spp.; colonization



**Citation:** Sabuquillo, P.; Cubero, J. Biofilm Formation in *Xanthomonas arboricola* pv. *pruni*: Structure and Development. *Agronomy* **2021**, *11*, 546. <https://doi.org/10.3390/agronomy11030546>

Academic Editors: Begonya Vicedo, Loredana Scalschi and Eugenio Llorens

Received: 25 January 2021

Accepted: 11 March 2021

Published: 13 March 2021

**Publisher's Note:** MDPI stays neutral with regard to jurisdictional claims in published maps and institutional affiliations.



**Copyright:** © 2021 by the authors. Licensee MDPI, Basel, Switzerland. This article is an open access article distributed under the terms and conditions of the Creative Commons Attribution (CC BY) license (<https://creativecommons.org/licenses/by/4.0/>).

## 1. Introduction

*Xanthomonas* is a large genus of Gram-negative bacteria that encompasses species that cause diseases in plants, including many economically important crops [1,2]. Within the *Xanthomonas* genus, many strains infect herbaceous and woody plants [3], with *Xanthomonas arboricola* pv. *pruni* (Xap), causal agent of bacterial spot disease on *Prunus* spp, being one of the most important pathovars [4]. Xap is distributed in Asia, Africa, North and South America, Oceania and Europe, where it has been recently re-classified from quarantinable to a regulated organism by the European Union [5].

Xap causes damages on leaves, fruit, twigs, branches and trunks of trees [6] and gradually heavily infected trees become uneconomic because of severe defoliation resulting in weakened trees and damaged fruit which are often unmarketable. Yield losses of up to 75% have been reported in orchards of peach fruit [7].

Biofilms are structural communities which consist of aggregates of bacterial cells encompassed by a protective polymeric matrix which facilitates their survival in adverse environments and plays key roles in infection and host colonization [8,9]. Biofilms are normally highly hydrated structures containing 73 to 98% extracellular and non-cellular material in addition to bacterial cells [10]. Multicellular behavior of the biofilms requires a certain population size and usually quorum sensing type mechanisms [11] which involves intercellular communication and signal transmission, as well as successful exchange of genetic information [12]. This information exchange comprises of specific signal molecules which ensure that the microbial community reacts as a single organism. Biofilm formation includes attachment and reversible adhesion of planktonic cells to the host surface, which

turns on an irreversible adhesion followed by formation of a monolayer with extracellular polymeric substance (EPS) secretion. Finally, biofilm maturation and the development of a three-dimensional structure occur, and at this point some cells disperse and become planktonic [13,14].

The ability of microorganisms to form biofilms on biotic and abiotic surface causes numerous problems in human health [15,16] and in other areas of economic importance, including agriculture [17–19]. In plants, several bacterial species have been described to attach to surfaces and form biofilms and such aggregation has been associated with difficulties in disease management [18,20–22]. Biofilms constitute a protected mode for the bacteria that allows them to survive in unfriendly environments, often being difficult to eradicate. Therefore, the need for developing control strategies based on the knowledge of these structures and the different elements conforming them is paramount [18].

In addition to biofilm formation, early stages of bacterial infection include processes like chemotaxis, cell motility or quorum sensing activated through sensors and receptors that detect stimuli and provide the cells with environmental information [23,24]. Bacterial appendages such as surface projections, flagella and pili, participate in reversible or non-reversible attachment, aggregation, and motility, which is also linked to biofilm formation [25]. Modulation of EPS production, associated with biofilms, is an adaptive mechanism that enables survival under stressful conditions. EPS provides stability and protects cells from antibacterial agents and damaging environmental factors, fixes the bacterial cells and is involved in recognition functions [26,27]. Moreover, hydrodynamics, nutrient concentration, carbon source, genetics, and quorum sensing have been identified as factors influencing biofilm architecture [28–30]. The presence of numerous, extensive membrane structures is another characteristic of bacteria in planktonic and biofilm conditions [31]. These structures mediate bacterial envelope stress, survival, colonization, biofilm nucleation and maintenance, virulence and transformation [32]. Xap is able to multiply epiphytically on leaf surfaces and forms biofilms that assist in the infection process. Moreover, ability of Xap to aggregate in host and non-host plants, has been compared with other xanthomonads causing similar symptoms in citrus [33,34].

Although the ability to form biofilm is a common attribute of bacteria, the mechanisms underlying this characteristic may vary depending on the species or even among specific strains and also according to the environment the cells occupy [35].

In this work, biofilm formation by Xap has been studied taking in account the nutrient content, the environment, and the population size on bacterial aggregation. Biofilms were analyzed using microscopy techniques which have allowed a detailed examination of the components involved in the formation of structures which enable the bacteria to adapt and response to stress.

## 2. Materials and Methods

### 2.1. Bacterial Strains and Media

The Xap strains used in this study were CITA 33 isolated from *Prunus amygdalus* cv. Guara, IVIA 2626-1 from *Prunus salicina* cv. Fortuna, IVIA 2832-10b from *P. salicina* cv. Angeleno, and IVIA 3161-2 from *Prunus amygdalus* cv Rumbeta. These strains were all isolated in Spain and selected according to the host and on the basis of the different phenotypic features described in previous work [36].

All strains were grown at 27 °C for 72 h in Luria Bertani (LB) broth (10 g L<sup>-1</sup> tryptone, 5 g L<sup>-1</sup> yeast extract and 5 g L<sup>-1</sup> sodium chloride) used as a common nutritional medium or on agar plates of LB (1.5% agar). Other culture media assayed were PYM (5 g L<sup>-1</sup> peptone, 3 g L<sup>-1</sup> yeast, 3 g L<sup>-1</sup> malt extract, 55 mM glucose), MMA (40 mM K<sub>2</sub>HPO<sub>4</sub>, 22 mM KH<sub>2</sub>PO<sub>4</sub>, 0.4 mM MgSO<sub>4</sub> 7H<sub>2</sub>O, 7 mM (NH<sub>4</sub>)<sub>2</sub>SO<sub>4</sub>, 2 mM sodium citrate, 22 mM glycerine), M9 (2 mL MgSO<sub>4</sub> 1 M, 20% glucose, 1 M CaCl<sub>2</sub>, 200 mL of a solution contained 0.2 M Na<sub>2</sub>HPO<sub>4</sub>, 0.086 M KH<sub>2</sub>PO<sub>4</sub>, 0.04 M NaCl and 0.093 M NH<sub>4</sub>Cl) and XVM2 (20 mM NaCl, 10 mM (NH<sub>4</sub>)<sub>2</sub>SO<sub>4</sub>, 5 mM MgSO<sub>4</sub>, 0.5 mM CaCl<sub>2</sub>, 0.16 mM KH<sub>2</sub>PO<sub>4</sub>, 0.32 mM K<sub>2</sub>HPO<sub>4</sub>, 0.01 mM FeSO<sub>4</sub>, 10 mM fructose, 10 mM sucrose, 0.03% casamino acids), a culture medium

that mimics apoplastic conditions [37]. LB agar was supplemented with cycloheximide 2% (*w/v*) in assays with plant material.

## 2.2. Growth of Xap Strains in Culture Media with Different Composition

Overnight bacterial cultures were centrifuged 15 min at 4000 rpm and washed twice with the same volume of 10 mM MgCl<sub>2</sub>. The bacterial pellet was finally suspended in LB, PYM, MMA, M9 or XVM2 media with a final concentration of 0.05 OD<sub>600</sub>. 300 µL of bacterial suspension were deposited into each well of a 100-well microplate (Oy Growth Curves Ab LTD, Turku, Finland). The growth rate of the Xap strains was measured in a Bioscreen C apparatus (Oy Growth Curves Ab LTD, Turku, Finland) at 27 °C, low speed and setting for 47 h with reads each hour at 600 nm. Three independent assays were performed, each including four replicates per culture. Areas under growth curves were calculated from OD (Optical Density) measurements at 600 nm.

## 2.3. Biofilm Formation and Quantification

Bacterial adhesion and biofilm formation were measured using a polypropylene 96-well plate assay as previously described [20,38]. 150 µL of an overnight bacterial suspension, processed as described above, were deposited into each well and incubated at 27 °C under static or shaking conditions for the time indicated in each plot. After this incubation time, the medium from the static cultures was carefully removed by micropipetting and deposited bacteria were incubated for an additional 72 h at 27 °C in static conditions (dry conditions in order to mimic early bacterial colonization of surfaces). Cell adhesion to the well surface was estimated spectrophotometrically by staining the adhered bacteria with crystal violet (CV, Merck KGaA, Darmstadt, Germany). Briefly, wells were carefully rinsed with sterile distilled water (SDW) and stained with 0.3% CV for 15 min. Excess stain was removed and the wells rinsed again with SDW. The remaining CV was solubilized by the addition of 150 µL of 20:80 acetone:ethanol and quantified using a microplate reader at 570 nm (Labsystems Multiskan RC spectrophotometer, Fisher Scientific, Waltham, MA, USA). Absorption values for each strain were calculated as the means of three readings of five wells from three independent assays. For each well the blank absorbance, without inoculum, was subtracted.

## 2.4. Statistical Analysis

Growth and biofilm data were analyzed using Statgraphics Centurion XVI.II version 16.2.04. The means were compared by analysis of variance (ANOVA) according to Student-Newman-Keuls (SNK) multiple range test. *p* = 0.05 was considered statistically significant.

## 2.5. Survival Assay In Vitro and “Ex Vivo”

Two assays were carried out to assess biofilm viability in vitro. First, viability of the aggregates was evaluated on LB culture plates. Xap 48 h mature biofilms, generated as described above, were removed from the polypropylene 96-well plates by adding 100 µL of SDW to each well containing Xap aggregates. These suspensions were plated onto LB petri dishes and after 2–3 days incubation at 27 °C, Xap-like colonies were recorded. Second, cellular respiration was assessed to confirm the viability of aggregates by alamarBlue (Bio-Rad Laboratories, Inc. Hercules, CA, USA). 72 h after medium removal from the polypropylene 96-well plates, 100 µL of SDW and 10 µL of alamarBlue reagent were added to each well containing Xap aggregates. The samples were incubated in darkness at 27 °C and those that turned from blue to pink were considered positive as respiration activity was detected. Both assays were repeated twice.

To verify Xap survival on leaf surface, an assay was performed on young detached leaves of different *Prunus* species: apricot (cv. Canino), peach (cv. Calanda) European plum (cv. Golden Japan) and almond (cv. Ferraduel). Leaves were washed three times in SDW and surface sterilized with 70% ethanol and 0.5% sodium hypochlorite. Then, the leaves were rinsed three times with SDW and dried in a hood. Eight leaves per host were selected

and inoculated with CITA 33 strain; sterilized leaf undersides were inoculated using a cotton swab impregnated with 10 mM  $\text{MgCl}_2$  (control) or with a bacterial suspension of CITA 33 in  $\text{MgCl}_2$  adjusted to 0.1  $\text{OD}_{600}$ . Inoculated and control leaves were deposited by the upper side onto agar-water (0.5%) petri dishes and incubated in a grow chamber at 27 °C, 80% HR with cycles of light of 12 h. Moreover, at 4, 10, 17, and 25 days post-inoculation (dpi), the underside leaves were incubated on LB agar plates supplemented with cycloheximide. Three days later, Xap colonies which appeared on the plates from infected leaves were recorded. The assay was repeated once.

## 2.6. Visualization of Biofilm Progression and Structures Involved

Strains were grown onto inert surfaces as previously described. To visualize the different structures involved in aggregation and biofilms, different microscopy techniques were used.

Glass slides or copper grids (Formvar/carbon coated-copper 400 mesh) were impregnated directly with CITA 33 grown on LB petri dishes or 20  $\mu\text{L}$  of CITA 33 suspension was deposited on them. Both preparations were incubated in a sterilized humidity chamber. For biofilm formation, initial cultures were removed and the slides or grids incubated under static conditions at 27 °C for an additional time according to the plot.

The biofilm structure formed on the glass slide was stained with 15  $\mu\text{L}$  of 1% *w/v* crystal violet [39] and analyzed under light microscopy with a Leica DMR modular stereo microscope equipped with a Leica DC 500 camera and Leica IM500 version 1.2 software for image acquisition (Leica microsystems, Wetzlar, Germany). The planktonic bacteria assay was evaluated as above for biofilms but without the culture medium removal step.

Biofilm architecture in different media was also visualized by a confocal laser scanning microscopy (CLSM, model TCS-NT; Leica, Germany). Samples of strain CITA33 grown in LB or XVM2 media and adhered to glass slides were stained with SYTO 9 following manufacturer's instructions (Life Technologies, Eugene, OR, USA). Images were acquired with an excitation/emission light of 485/498 nm, 40 $\times$  objective lens and processed using Adobe PhotoShop 6 software (Adobe, Mountain View, CA, USA).

Ultrastructural analysis was performed by transmission electron microscopy (TEM) to reveal the cell interaction traits. CITA 33 grown on LB petri dishes or 20  $\mu\text{L}$  from CITA 33 suspensions were deposited on Copper grids (Formvar/carbon coated-copper 400 mesh) following the protocol described above. For negative staining, 5  $\mu\text{L}$  of 1% of uranyl acetate were added onto the sample for 1 min and air dried in a hood. Images were visualized and recorded in a JEOL JEM 1010 at 100 kV with a BL6 thermionic electron tube and a megaview II camera, with a resolution between points of 0.35 nm (National Centre of Electron Microscopy, ITCS-CNME, Madrid, Spain).

Analysis of Xap on biological surfaces was achieved by scanning electron microscopy (SEM). Leaves and fruit from apricot, peach, plum, and almond previously sterilized were inoculated with strain CITA 33 as described above. Pieces of inoculated leaves or the fruit rind (<6 mm) were fixed in 3% glutaraldehyde in 0.1 M  $\text{KPO}_4$  buffer, then post-fixed in 2%  $\text{OsO}_4$  in 0.1 M  $\text{KPO}_4$  buffer. After washing with SDW, samples were dehydrated by increasing concentrations of ethanol and critical point dried with  $\text{CO}_2$ . The samples were mounted on metal stubs and coated in gold/palladium. Samples were examined in a JSM 6400 microscope at 25 kV (National Centre of Electron Microscopy, ITCS-CNME, Madrid, Spain).

## 3. Results

### 3.1. *Xanthomonas Arboricola* pv. *Pruni* Growth in Different Conditions

The study was initially focused on the influence of bacterial growth on bacterial aggregation and biofilm formation in different nutrient conditions.

Growth of several Xap strains was analyzed in culture media with different nutrient content: LB and PYM with a high nutrient content, MMA and M9 minimum media with

low nutrient content, and XVM2 a low nutrient content medium that mimics plant leaf apoplast condition (Figure 1).

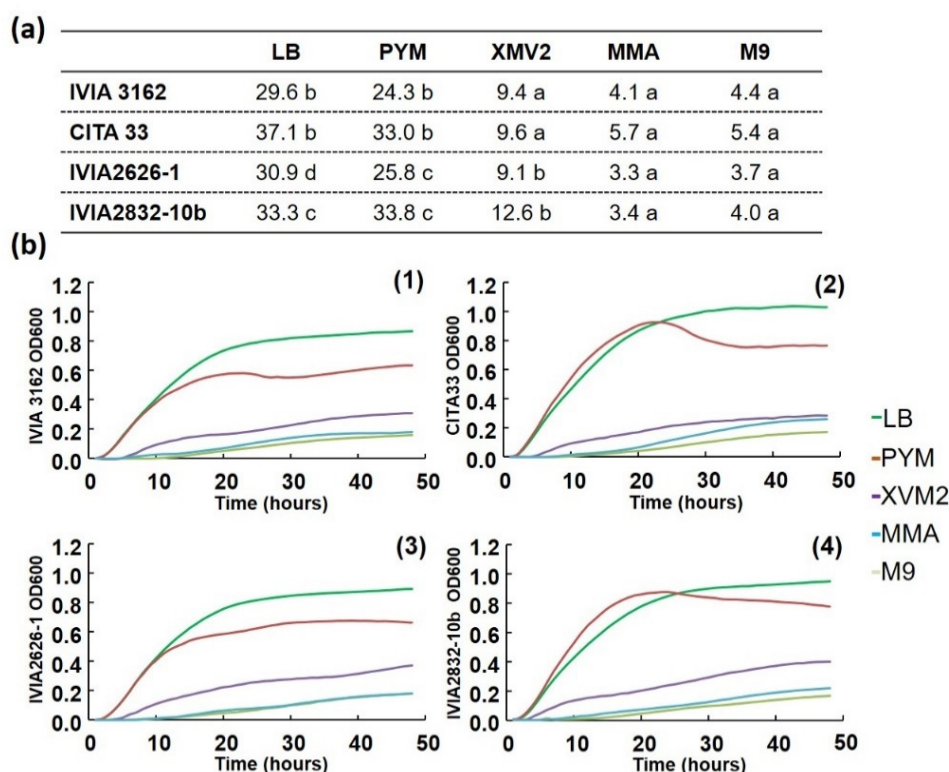


**Figure 1.** (a) Areas under growth curves ( $OD_{600}$ ) of Xap strains on: LB, PYM, MMA, XVM2 and M9 media. The table shows the average of four replicates in each two assays. Means with the same letter in a row do not differ significantly according to Student-Newman-Keuls test ( $p = 0.05$ ). (b) Measure of bacterial growth by absorbance at 600 nm. Media assayed: LB, PYM, MMA, XVM2 and M9. Xap strains: IVIA 3162 (1), CITA 33 (2), IVIA 2626-1 (3) and IVIA 2832-10b (4).

All the strains assayed reached the highest  $OD_{600}$  in LB or PYM media and the lowest in MMA and M9. For most of the strains, no differences were recorded between the two high nutrient content media, LB and PYM, but clear differences were observed between them and the apoplast mimicking medium or with the low nutrient content media. Bacterial growth in XVM2 did not differ significantly or showed only small differences compared to MMA and M9 minimum media (Figure 1a). Bacteria in a high nutrient culture media, LB or PYM, have shorter lag phase and reached the exponential (log) phase before than those in low nutrient media (Figure 1b). After 50 h growth, all strains in all media, reached the maximum OD, and remained stable until 144 h when the bacterial concentration declined (results not shown).

### 3.2. Bacterial Aggregation and Biofilm Formation of Different Xap Strains

To evaluate biofilm formation of the different Xap strains, diverse culture media and nutrient conditions were evaluated in relationship to bacterial growth rate.

The influence of culture media, and therefore, the effect of nutrient content on biofilm formation for each Xap strain, is shown in Figure 2.



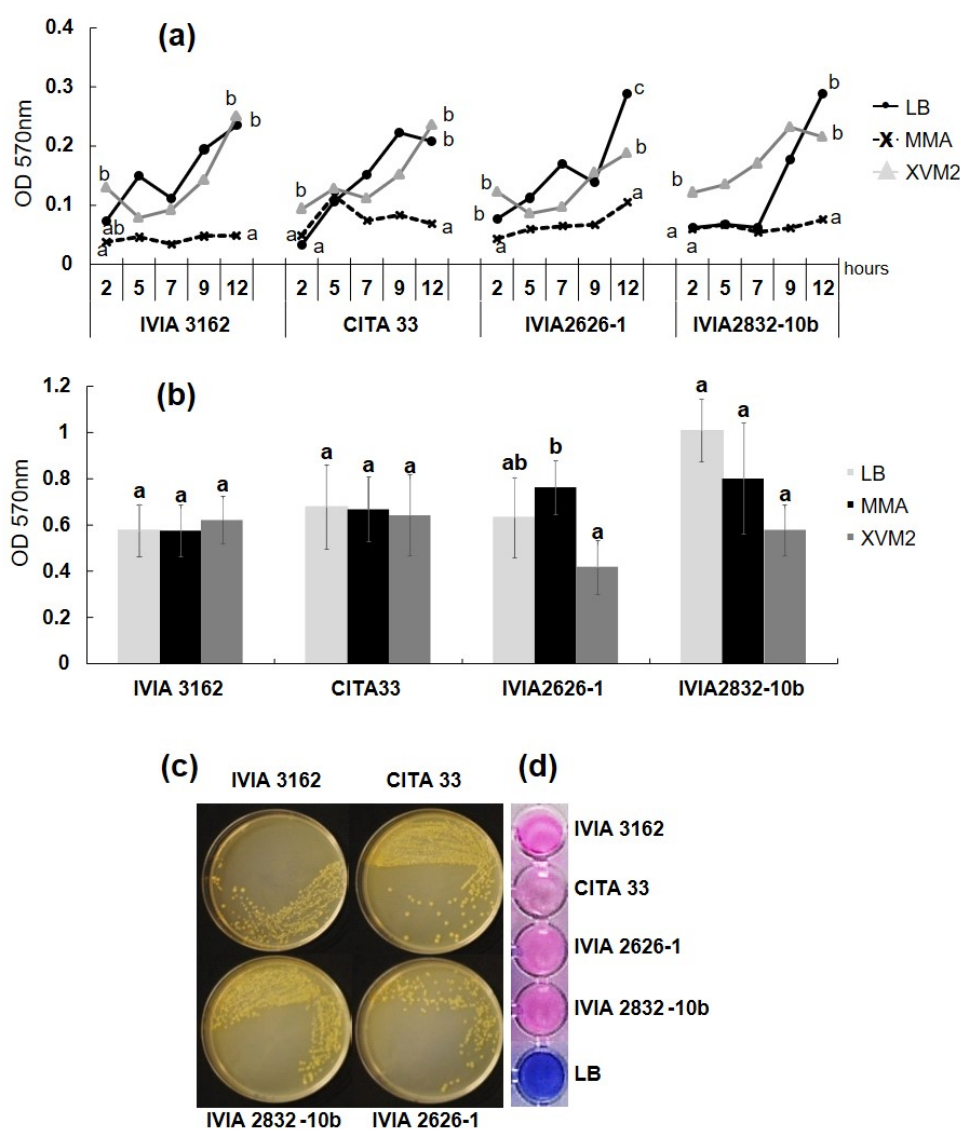


**Figure 2.** (a) Biofilm formation by Xap on polypropylene surface quantified by absorbance (570 nm) of crystal violet stain. Biofilm recorded at different growth times (from 2 to 12 h) in LB, MMA and XVM2 media after 72 h in static and dry condition (72 h incubation with no culture medium). (b) Biofilm recorded at 144 h of Xap growth and quantified in LB, MMA and XVM2 at 570 nm. (c) Bacterial colonies resulted from cells recovered from 48 h mature biofilm on LB. (d) Detection of cellular respiration with alamarBlue reagent of different Xap strains and negative control (LB). Blue color denotes no viable cells and pink color viable cells. Means with the same letter within the same time (a) or strain (b) do not differ significantly ( $p < 0.05$ ).

Xap strains formed more biofilm in LB and XVM2 compared to MMA medium from 2 h to 12 h (Figure 2a). Aggregation progression was faster in LB as compared to XVM2 in this timeframe. Greater initial bacterial attachment was revealed in XVM2 at the beginning of the process (2 h) but similar or more aggregation was achieved on LB at the end (12 h). At 144 h of bacterial growth, when all cultures had reached the maximum population for the bacteria, no significant differences on biofilms were found among the different culture media tested (Figure 2b). Overall, all strains showed similar behavior either in early stage of the biofilm (Figure 2a) or mature biofilm (Figure 2b).

To assess if Xap aggregates were composed of living and active cells, and therefore were real biofilms and not simple physical cell aggregates, two assays were carried out, one based on the bacteria ability to grow in culture media and the other based on cellular respiration. As shown in Figure 2c, cells recovered from 48 h mature biofilm grew in

colonies on nutritive medium indicating the viability and culturability of these aggregates. In addition, cellular respiration of the different Xap strains was evaluated after 72 h of biofilm formation in dry condition. All reactions from each strain tested turned from blue to pink, confirming cellular respiration and presence of viable cells in the bacterial aggregates (Figure 2d).

### 3.3. Visualization of Biofilms In Vitro

Biofilm progression was evaluated by different microscopy techniques. Bacterial aggregates were stained using crystal violet, SYTO and osmium tetroxide and observed by optical or electron microscopy.

Optical microscopy observation of planktonic and biofilm structure development of strain CITA 33, which was selected as a Xap representative strain, is shown in Figure 3a.

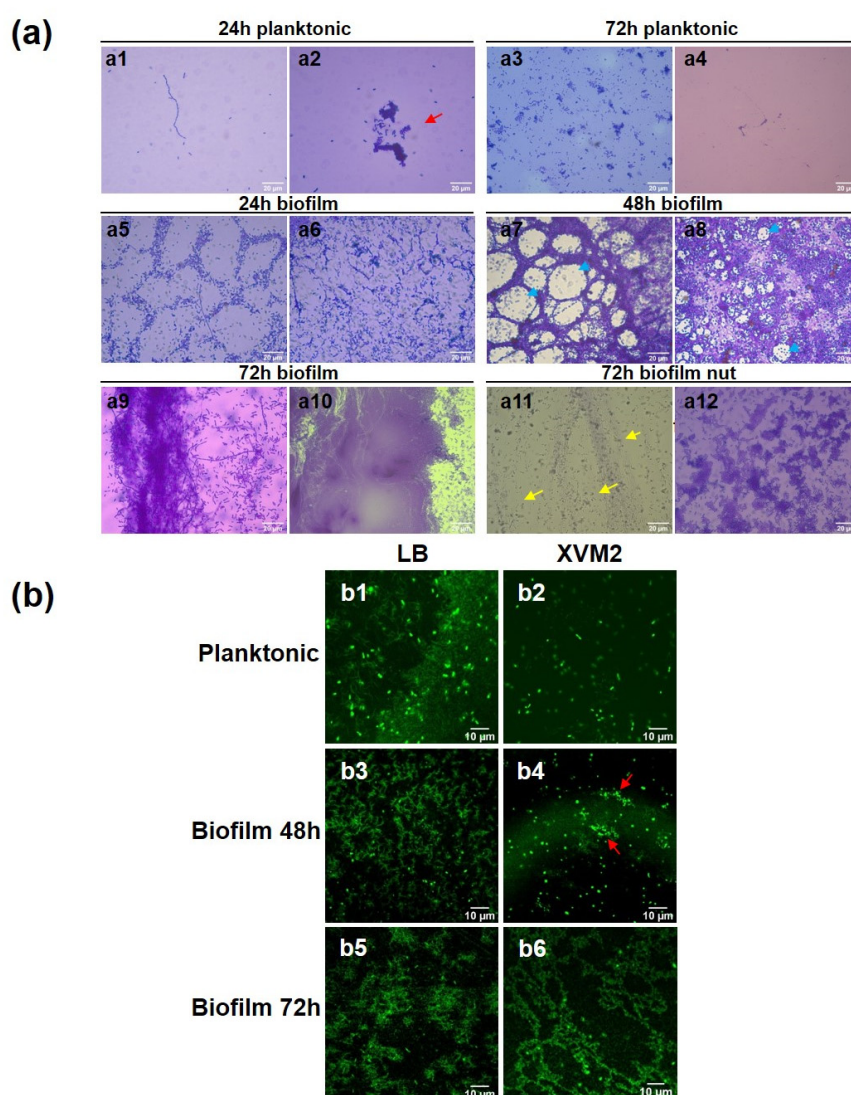


**Figure 3.** (a) Optical microscopy of morphological features of CITA 33 strain in LB medium. Samples were stained with crystal violet at different stage: 24 h of bacteria growth in shaking conditions (1,2), 72 h of bacteria growth in shaking conditions (3,4), 24 h of biofilm maturation in dried conditions (5,6), 48 h of biofilm maturation in dry condition (7,8), 72 h of biofilm maturation in dry conditions (9,10), 72 h of biofilm maturation without medium elimination (11,12). (b) CLSM imaging of planktonic cells in LB (1) and XVM2 (2), 48 h mature biofilm in LB (3) and XVM2 (4) and 72 h mature biofilm in LB (5) and XVM2 (6).

After 24 h growth under shaking, Xap formed cellular chains composed by aligned cells (Figure 3a: a1) in addition to small bacterial aggregates surrounded by a slight EPS-like matrix (Figure 3a: a2 and Figure S1: a, b, red arrows). After 72 h growth, some cells remained solitaires or forming lines (Figure 3a: a3, a4 and Figure S1: c, d), but small clusters were more profuse and the matrix more abundant.

Figure 3a: a5 to a10 and Figure S1: e to j show the progression from early stage of bacterial aggregation to mature biofilm after medium removal. Xap showed a clearly defined structure with masses of cells in a honeycomb configuration (Figure 3a: a5, a7 and Figure S1: e, i). Bacterial lines were observed, being more abundant and thicker 72 h in dry condition (Figure 3a: a9 and Figure S1: j). Moreover, at this time, a dense aggregation encompassed by cellular multilayers was shown (Figure 3a: a10). The staining of clumped cells, in dark blue, was observed at early (24 h) and at medium (48 h) stage of biofilm maturation (Figure S1: f, h). A matrix was shown in every step of the maturation process, being denser at longer during biofilm maturation. This matrix material seemed to serve as the skeleton of biofilm structure (Figure 3a: a6, a8 and Figure S1: g) where bacterial cluster trapped in voids were encompassed (Figure 3a: a7, a8 and Figure S1: j, blue arrows). When the study was performed without medium elimination (Figure 3a: a11, a12 and Figure S1: k, l), the aggregation was less dense, but still structured with production of matrix material and fibers (Figure 3a: a11, yellow arrows).

When the different structures were analyzed by CLSM in liquid media, planktonic cells were mainly solitary either in LB or XVM2 media (Figure 3b: b1, b2). 48 h mature biofilm in LB exhibited, in addition to dispersed cells, a compacted and defined structure (Figure 3b: b3). When the medium was XVM2 that mimics the apoplastic condition, dispersed cells prevailed, but an initial biofilm structure was also detected (Figure 3b: b4, red arrows). A highly dense structure was observed in LB medium with few dispersed cells 72 h after medium removal (Figure 3b: b5). In XVM2, a structure less condensed than in LB was recorded in addition to dispersed cells (Figure 3b: b6).

Ultrastructural analysis by transmission electron microscopy (TEM) revealed details of Xap aggregation on LB plates, at planktonic and biofilm stages (Figure 4).

Xap assembled in an organized structure (Figure 4: a1, c1 and Figure S2: a1, b3, c1) and a cellular tapestry was predominant in the structure after 72 h biofilm maturation (Figure 4: c3 and Figure S2: c2, c3). Clusters of amorphous, deformed and intimately joined cells surrounded by EPS preserving the honeycomb structure were recorded at 24 h and 48 h of aggregation in static conditions (Figure 4: c1 and Figure S2: c1). In addition to cellular clusters submitting larger bunches and branched fibers connecting bacterial groups (Figure 4: b2, c2), thin fibers that serve as bacterial support, connecting and covering cells (Figure 4: a2 and Figure S2: a1, b3), and individual fibers emission were visualized (Figure 4: a3, b1, b3 and Figure S2: a2, b1, b2, b3). Vesicles-like particles production from the cell (green arrows), in addition to tiny spherical particles (red arrows), were also observed (Figure 4: a3, b3 and Figure S2: a2, a3). No observable difference was recorded from 24 h to 72 h of aggregation in shaking conditions. In all circumstances, Xap presented cells with different sizes and dividing cells.

Detailed study of cellular features and connections of Xap at different growth conditions are shown in Figure 5.



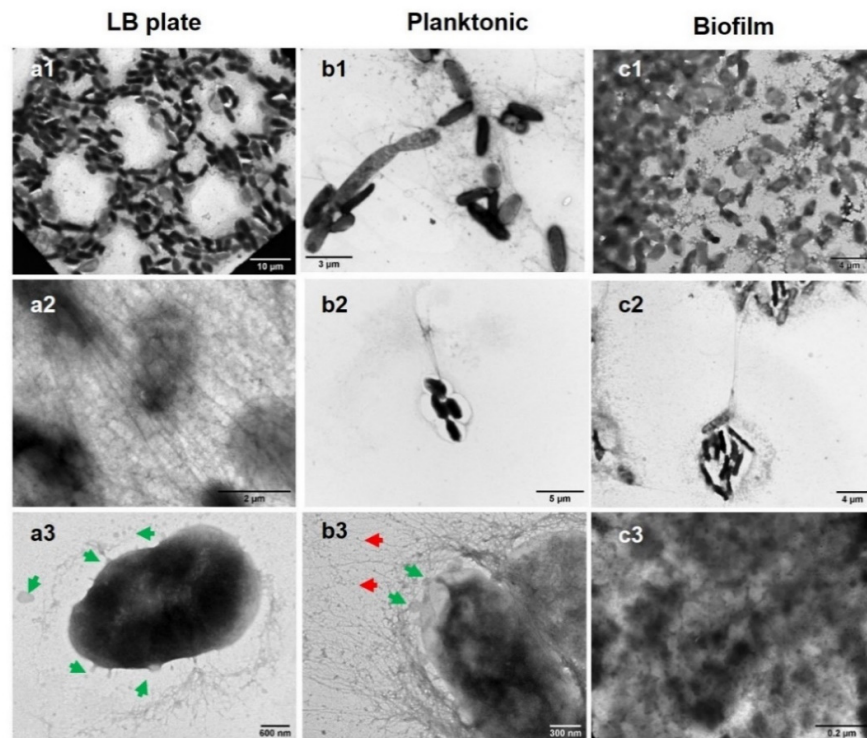


**Figure 4.** Ultrastructural analysis by TEM of the aggregation of CITA 33 strain in LB medium on petri plate in static conditions at 72 h growth (a1–a3). Progression of planktonic cells in LB liquid culture at 24 h (b1) and 72 h growth (b2,b3). 48 h (c1,c2) and 72 h (c3) mature biofilm.

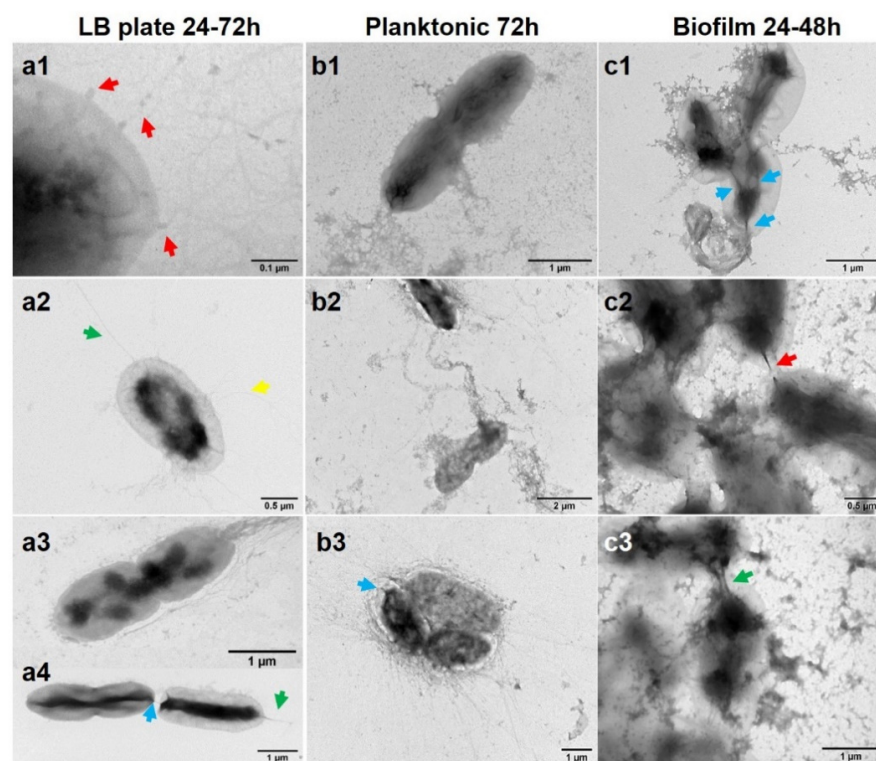


**Figure 5.** TEM analysis of cellular feature of CITA 33 cells in LB medium. On petri plate in static conditions at 24 h (a1) and 72 h (a2–a4) growth. Planktonic cells in liquid culture at 72 h (b1–b3) growth. 24 h (c1) and 48 h (c2, c3) mature biofilm.

A variety of filamentous structures in association with spherical particles (Figure 5: a1 and Figure S3: a1) or projected from the bacteria such as lateral and/or polar fibers (Figure 5: a2, a4, yellow and green arrows, respectively), thick with branches (Figure S3: a2, b2), in a bouquet (Figure 5: a3) or individual fiber joining cells (Figure 5: a4, blue arrow), were observed. EPS projections connecting cells were also recorded (Figure 5: b2). Heterogeneous cytoplasm distribution along the cell or located at the poles were observed (Figure 5: a2, a3, b1, c1 and Figure S3: a1, b1, c1). In addition to expelling cytoplasmic material (blue arrows) from the bacteria (Figure 5: b3 and Figure S3: a3, b3, c1), cytoplasmic like-finger projections that may interconnect cells, were recorded (Figure 5: c1, blue arrows). Those projections showed different looks: thin (Figure 5: c2 and Figure S3: c3, c4, red arrows), double (Figure 5: c3, green arrow) or thick (Figure S3: c2, yellow arrow).

Different structures visualized at planktonic and biofilm stages are shown in Figure 6.

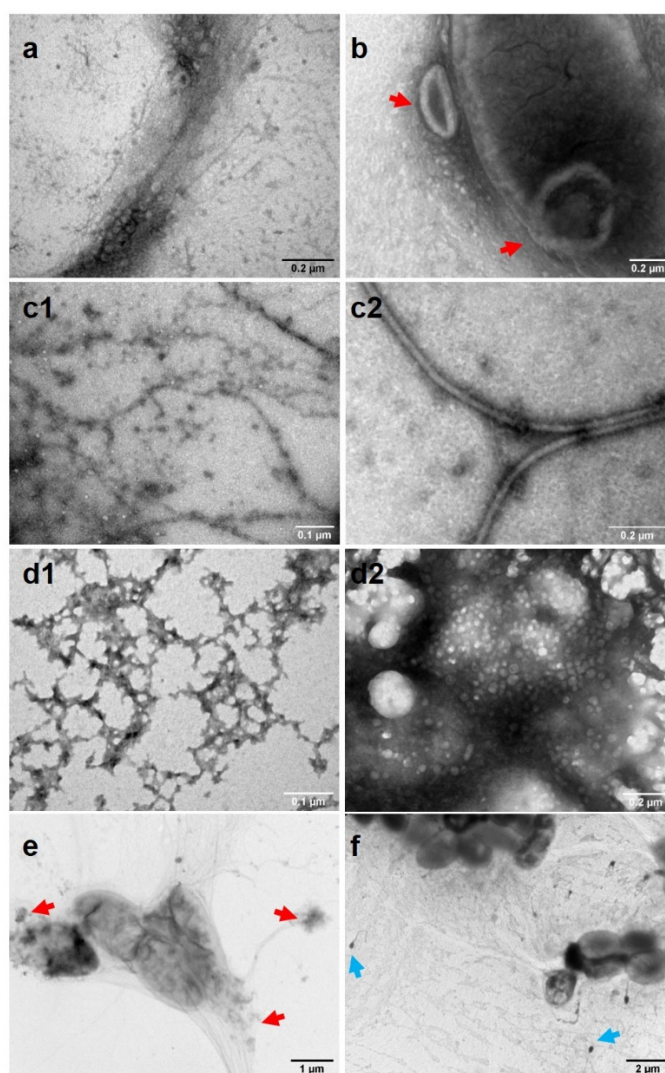


**Figure 6.** Structures recorded by TEM at planktonic stage and during CITA 33 biofilm progress. Putative vesicles (a), membranes (b), fibers feature (c1,c2), EPS feature (d1,d2), broken cells (e) and putative phages (f).

Particles compatible with vesicles presenting different sizes, dispersed or forming groups along a fiber, were detected in planktonic and biofilm stages (Figure 6: a and Figure S4: a1, a2). Membranes associated with bacterial cells (Figure 6: b and Figure S4: b1, b2, red arrows) and different types of fibers in association with spherical particles were recorded (Figure 6: c1, c2 and Figure S4: c). The structure of EPS alone (Figure

6: d1 and Figure S4: d) or enclosing particles compatibles with vesicles (Figure 6: d2) is shown. Broken cells expelling abroad their inner content (Figure 6: e, red arrows), or with putative vesicles inside and outside (Figure S4: e, yellow arrows). The presence of particles compatible with phages is shown in Figure 6: f (blue arrows).

### 3.4. Visualization of Biofilm Ex Vivo

Colonization of Xap on a biotic surface is shown in Figure 7. Detached leaves of apricot, almond, cherry, plum and peach trees were inoculated with a suspension of CITA33 strain and its progression monitored at different time points. All the leaves inoculated showed that at 9 dpi the surface was coated with EPS that seems to increase over the time. Solitary or grouped bacteria attached to the underlying surface by fimbria-like appendages (red arrows). In addition, the number of collapsed stomata increased over the time, especially at 30 dpi in plum leaves (yellow arrows). Other types of fibers with different shapes (green arrows) and spherical particles (blue arrows) in association with them, were observed during the time period of the assay. Visualization of individual or grouped cells was difficult as the bacterial colonization progressed, due to the abundance of the biofilm matrix.

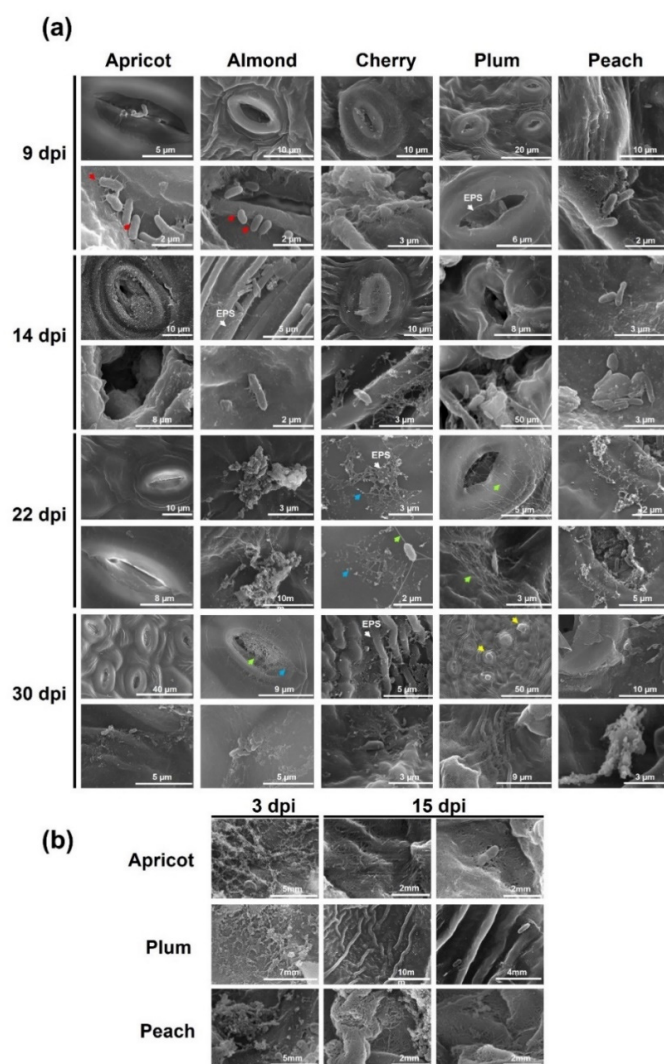


**Figure 7.** SEM analysis of colonization of CITA 33 strain on detached leaves of apricot, almond, cherry, plum and peach tree (a) and on detached fruit of apricot, plum and peach (b) at different days of bacterial post-inoculation (dpi).



Connection structures among cells observed on detached leaves were similar to those shown on fruit (Figure 7b). A complex and organized structure was observed mainly conformed of fibers and appendages from the bacteria, as well as an EPS matrix. In this structure, bacterial cells were at times difficult to differentiate from the biofilm matrix and plant material.

Survival of Xap on biotic surfaces was evaluated by footprinting onto LB medium. Xap cells were recovered from surface of detached leaves of plum, apricot, almond, and peach from 4 to 25 dpi, even if symptoms appeared at 25 dpi (Figure 8).

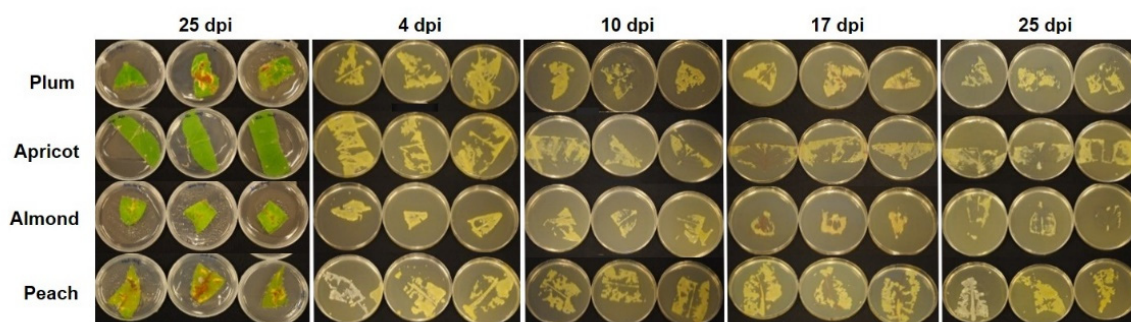


**Figure 8.** CITA 33 biofilm viability ex vivo. Imprints of detached leaves from plum, apricot almond and peach on LB medium at 4, 10, 17 and 25 dpi. First column showed the symptoms 25 dpi.

#### 4. Discussion

Bacterial biofilm represents one of the major mechanisms that microbial communities use to adapt to environmental changes, to survive and colonize plants. A biofilm is the result of complex coordinated interactions of microorganisms that form a multilayer of cells attached to a surface and to each other. In these communities the majority of the population is alive. The biofilm life cycle is initiated by the transition from a reversible to an irreversible attachment which is followed by cellular aggregation and maturation. The initial surface contact of the planktonic cells leads to complex cellular differentiation. Analysis of ultrathin sections demonstrated that unlike planktonic cells, in biofilms, morphologically altered bacteria are common [40].

Studies of biofilms from plant pathogenic bacteria belonging to the genus *Xanthomonas* have been already performed [41–44]. Moreover, the ability of Xap, the causal agent of bacterial spot of stone fruit, to adhere to abiotic and biotic surfaces and to form biofilms was evaluated [33]. In this study, the characterization of Xap in biofilms was analyzed and compared with planktonic communities of the bacteria under different nutrient conditions.

Nutrient availability is crucial for bacteria to ensure survival and successful host colonization. It is also known that bacteria modulate their machinery according to the niche and use different strategies, intimately related to their virulence mechanisms, to acquire nutrients [28]. The primary aim of this study was to determine the nutrient effect on growth rate and biofilm formation comparing high nutrient availability and nutrient limitation conditions. As expected, all Xap strains evaluated showed faster bacterial growth in nutritive media and lower in a low nutrient environment. Growth in XVM2, the medium which mimics apoplastic condition, was similar to that in media with low nutrient content. Bacterial populations declined, as expected, in all culture media after prolonged incubation due to nutrient deprivation that would be the case if no virulence mechanisms are activated to release nutrient elements from the plant host during the infection process as occurred in the in vitro growth assays.

Bacterial adhesion is a complex process modulated by many factors, such as the molecules released by the bacteria [45,46], the hydrophobicity of the surface [14,47,48], and environmental surroundings [49] that may attract the cells to adhere to a surface, favoring the deposition of other bacteria which multiply and promote an increase in biomass. All



Xap strains evaluated were able to form real biofilms as revealed by aggregation and viability assays. In our study, the influence of the bacterial population level achieved under different nutrient conditions was tested on biofilm formation. Higher aggregation was observed in a high nutrient content environment, in agreement with that found in *Pseudomonas* [48], but contrary to what occurs in *Xanthomonas citri* subsp. *citri* (Xcc) that stimulated aggregation and biofilms in an apoplastic-like environment [20]. This different behavior between Xcc and Xap could be related to their different infection modes and the distinct biofilm role on it. Biofilms in Xap seems to be a priority to establish and colonize the host in its epiphytic phase but inside the plant, within the apoplast, may not be as crucial as in Xcc [34]. To refine the understanding of the plant-Xap interaction it is needed to go further performing new studies on other nutritional conditions or including different parts of the plants.

In *Pseudomonas fluorescens*, adhesion occurs through proteins at the cell polar region (CPR) and the formation of a cell monolayer involved cell fission, cell separation, lateral movement of the new cell apices, and sliding of these apices past one another [23]. In our study, cells were orientated by their polar region (apical links) and long queues of Xap cells were shown either in planktonic or biofilm states. TEM images suggest that the initial reversible cell adhesion could be mediated by fimbria pili structures in additions to other types of appendages, mainly located at the CPR. Moreover, cells sharing cytoplasmic substance with different densities inside the cell were recorded in Xap. This feature could be related with a major biofilm compaction and bacterial communication in order to achieve better community survival. As far as we know, this is the first work where apical links and cytoplasmic rearrangement have been observed in the genus *Xanthomonas*.

The production of EPS matrix has been related with the promotion of cell aggregation [50], being a critical step for the multicellular assembly, the spatial and temporal distribution of different matrix constituents during cell adhesion and during biofilm maturation [14]. In our work, we recorded Xap producing EPS matrix at the very early stages of culture, progressing during biofilm development to cover the cells, both in abiotic and biotic conditions. The microscopy analyses support Xap biofilm architecture changes depending on the culture medium, being less dense structures in XVM2 than LB medium. This modification of biofilm architecture, related with changes in habitats, has already been demonstrated in different bacteria [51–53]

Clusters have been defined as main units of the biofilm architecture [54]. Herein, small clusters that might contribute to the monolayer structure that progress to a compact multilayer structure, were identified. Janissen et al. [14] confirmed bacterial clusters and their gradual interconnection increases due to a dramatic phenotypic change consisting of an elongation of a few cells located at cluster boundaries. These changes in cellular size have been also described in other bacterial genera [47,55,56]. In our study, elongated cells of Xap and cells with different sizes were shown in planktonic and biofilm stages. Moreover, it is remarkable the presence of elongated cells and EPS matrix on the surface of the *Prunus* species often resulting in collapsing stomata. We hypothesize that the existence of diverse cell morphologies may be related with their different roles into the community at different bacterial stages.

Production of fibrillar material connecting or not the neighboring was observed [40,57]. Serra et al. [58] described that *Escherichia coli* may produce two types of fibers during biofilm formation, flagella and curli. Diverse amyloid fibers produced by different bacterial and some of them identified as bacteriophages sequesters have been also described [59]. Moreover, the curli assembly was associated with spherical particles such as outer membrane lipoproteins [60]. In our studies, Xap cells exhibited diverse fibrillar material connecting cells in association with tiny spherical particles. These structures were noted at the planktonic stage and on biotic surfaces, but they were not as abundant at the biofilm stage. Further studies are needed to characterize the nature of these fibers in order to determine their different roles in the infection process.

Rigano et al. [61] demonstrated that Xcc formed a tight structure packed in hexagonal arrays separated by water-filled channels. These channels and biofilm porosity might facilitate the distribution of nutrients, oxygen, water and detritus flux throughout the biofilm [10,62]. Lawrence et al. [63] described types of motility for surface colonization different from gliding or flagellar motility, such as packing, spreading, shedding, and rolling maneuvers associated with the formation of microcolonies with spaces in their structure. Davey et al. [11] and Webb et al. [64], demonstrated that water channels in *P. aeruginosa* microcolonies were actively maintained by the quorum-sensing-controlled production of rhamnolipid surfactants. We hypothesize that Xap honeycomb structure shown in our work, could be the result of an EPS preformed complex and the specific cellular movement and site rearrangements that arise in a highly porous structure allowing better inter and intra cellular cooperation.

In biofilms some cells have an “altruist” behavior that lead to an increase in the fitness of the group [54,65]. This “altruist” behavior may be a consequence of an autolysis mechanism [66]. In other bacterial models endolysins produced by bacteriophages have been related to cell lysis with liberation of the cytosolic content [67,68]. In this study, we have observed broken bacterial cells releasing internal material, including, particles compatible with phages that may produce this cell lysis. Phages have been previously described in Xap and even used in biocontrol strategies for bacterial spot of stone fruit [69,70] and we hypothesize that might play a role in Xap biofilm formation contributing to this “altruist” behavior.

The presence of membrane structures is another characteristic of biofilms, these are associated with different production pathways [71] such as cell lysis, budding of LPS-containing outer membrane and cytoplasmic membrane origin connected with filamentous structures [72]. Bacterial extracellular vesicles (EV) are described to be heterogeneous in population and size as well as presenting different density, cargo content and variable production and distribution according to the physiological stage [73]. These vesicles may play key roles in multiple signaling pathways which start by their fusion with the plasma membrane to discharge their contents into the target cells [74]. They were also associated with defense mechanisms against phages [75]. Turnbull et al. [67] demonstrated that membrane vesicles (MV), derived from shattered membrane fragments produced as consequence of cell explosion, were formed via the curling and self-annealing of these membrane fragments. In our study, we have recorded different sizes of putative vesicles grouped or associated with fibers in planktonic and static conditions. Other structures implicated in Xap biofilm formation and observed/described here were circular and grouped membranes that may serve as a source of future vesicles, play a chemotaxis role or be a nutrient source for the bacterial population.

Biofilms stabilize bacterial colonization on the plant and provides protection from different stresses, and moreover participates in the virulence process [18]. Effective management of the biofilms is therefore a crucial challenge for bacterial control. This is the first study where different structures involved in biofilms have been identified in the genus *Xanthomonas* (Summarized in Table S1); this knowledge is essential in order to develop new control strategies for important diseases they cause, such as bacterial spot of stone fruit.

## 5. Conclusions

Xap is able to adhere to both biotic and abiotic substrates, eventually forming biofilms on them. During the biofilm formation, dense packing of the cells in a biofilm is accompanied by changes in cell shape and ultrastructural organization that may result in the bacteria adapting to the environment. Biofilm structure is formed a few days post-inoculation prior to the appearance of symptoms and may have important implications for disease control. To our knowledge, this is the first report about the structure, formation, and biofilm maturation of Xap and allows a deeper knowledge about the structures involved in biofilm formation of this plant pathogenic bacteria. This information is necessary in order to

develop novel and specific control methods for this important bacterial disease of *Prunus* spp. such the bacterial spot of stone fruit and almond.

**Supplementary Materials:** The following are available online at <https://www.mdpi.com/2073-4395/11/3/546/s1>, Figure S1. Optical microscopy of morphological features of CITA 33 strain in LB medium. Samples were stained with crystal violet at different stages: 24 h of bacteria growth in shaking conditions (a, b), 72 h of bacteria growth in shaking conditions (c, d), 24 h of biofilm maturation in dry conditions (e, f), 48 h of biofilm maturation in dry conditions (g, h), 72 h of biofilm maturation in dry conditions (i to j), 72 h of biofilm maturation without medium elimination (k,l). Figure S2. Ultrastructural analysis by TEM of the aggregation of CITA 33 strain in LB medium on petri plate in static conditions at 72 h growth (a1 to a3). Progression of planktonic cells in LB liquid culture at 24 h (b1, b2) and 72 h growth (b3). 24 h (c1) and 72 h (c2, c3) mature biofilm. Figure S3. TEM analysis of cellular feature of CITA 33 cells in LB medium. On petri plate in static conditions at 24 h (a1) and 72 h (a2, a4) of growth. Planktonic cells in liquid culture at 72 h (b1 to b3) of growth. 24 h (c1, c2) and 48 h (c3, c4) mature biofilm. Figure S4. Structures recorded by TEM at planktonic stage and during CITA 33 biofilm progress. Putative vesicles (a1, a2), membranes (b1, b2), fibers feature (c), EPS feature (d), broken cells (e). Table S1. Main structures found in the different bacterial stages over the length of the study.

**Author Contributions:** J.C. and P.S. conceived and designed the study as well as analyzed the data. P.S. performed most of the experimental work and prepared the first draft of the manuscript. Both authors reviewed the manuscript and both are considered corresponding authors. Both authors have read and agreed to the published version of the manuscript.

**Funding:** This work was supported financially by the Instituto Nacional de Investigación y Tecnología Agraria y Alimentaria (INIA) Ministerio de Ciencia Innovación y Universidades and Agencia Estatal de Investigación (AEI) from Spain, projects RTA2014-00018-C02-01 and RTI2018-096018-R-C31 cofinanced by FEDER.

**Institutional Review Board Statement:** Not applicable.

**Informed Consent Statement:** Not applicable.

**Data Availability Statement:** Not applicable.

**Acknowledgments:** We would like to thank to Ana Palacio-Bielsa (CITA, Aragón) and María M. López (IVIA, Valencia) for providing bacterial strains used in the study and Elisa Ferragud for her technical assistance. We would like also to thank Lee Robertson for English revision of the manuscript. The authors of the paper are members of the COST Action CA16107 EuroXanth: Integrating science on Xanthomonadaceae for integrated plant disease management in Europe. Facilities of the National Center for Electron Microscopy (CNME) of Universidad Complutense of Madrid, Spain, were used for SEM and TEM studies.

**Conflicts of Interest:** The authors declare no competing interests.

## References

- Hayward, A.C. The hosts of *Xanthomonas*. In *Xanthomonas*; Springer: Dordrecht, The Netherlands, 1993; pp. 1–119. ISBN 978-94-010-4666-4.
- Ryan, R.P.; Vorhölter, F.-J.; Potnis, N.; Jones, J.B.; Van Sluys, M.-A.; Bogdanove, A.J.; Dow, J.M. Pathogenomics of *Xanthomonas*: Understanding bacterium-plant interactions. *Nat. Rev. Microbiol.* **2011**, *9*, 344–355. [[CrossRef](#)] [[PubMed](#)]
- Lamichhane, J.R. *Xanthomonas arboricola* diseases of stone fruit, almond, and walnut trees: Progress toward understanding and management. *Plant Dis.* **2014**, *98*, 1600–1610. [[CrossRef](#)] [[PubMed](#)]
- Fischer-Le Saux, M.; Bonneau, S.; Essakhi, S.; Manceau, C.; Jacques, M.A. Aggressive emerging pathovars of *Xanthomonas arboricola* represent widespread epidemic clones distinct from poorly pathogenic strains, as revealed by multilocus sequence typing. *Appl. Environ. Microbiol.* **2015**, *81*, 4651–4668. [[CrossRef](#)]
- OJEU. Official Journal of European Union L41. *Off. J. Eur. Union L41* **2020**, *63*, 1–77.
- EFSA Scientific Opinion on pest categorisation of *Xanthomonas arboricola* pv. *pruni* (Smith, 1903). *EFSA J.* **2014**, *12*, 3857. [[CrossRef](#)]
- Stefani, E. Economic significance and control of bacterial spot/canker of stone fruits caused by *Xanthomonas arboricola* pv. *Pruni*. *J. Plant Pathol.* **2010**, *92*, 99–103.
- Flemming, H.C.; Wingender, J. The biofilm matrix. *Nat. Rev. Microbiol.* **2010**, *8*, 623–633. [[CrossRef](#)]

9. Gloag, E.S.; Fabbri, S.; Wozniak, D.J.; Stoodley, P. Biofilm mechanics: Implications in infection and survival. *Biofilm* **2020**, *2*, 1–10. [[CrossRef](#)]
10. Lawrence, J.R.; Korber, D.R.; Hoyle, B.D.; Costerton, J.W.; Caldwell, D.E. Optical sectioning of microbial biofilms. *J. Bacteriol.* **1991**, *173*, 6558–6567. [[CrossRef](#)]
11. Davey, M.E.; O’toole, G.A. Microbial biofilms: From ecology to molecular genetics. *Microbiol. Mol. Biol. Rev.* **2000**, *64*, 847–867. [[CrossRef](#)] [[PubMed](#)]
12. Romanova, I.M.; Smirnova, T.A.; Andreev, A.L.; Il’ina, T.S.; Didenko, L.V.; Gintsburg, A.L. Formation of biofilms as an example of the social behavior of bacteria. *Mikrobiologia* **2006**, *75*, 481–485. [[CrossRef](#)]
13. Stoodley, P.; Wilson, S.; Hall-Stoodley, L.; Boyle, J.D.; Lappin-Scott, H.M.; Costerton, J.W. Growth and detachment of cell clusters from mature mixed-species biofilms. *Appl. Environ. Microbiol.* **2001**, *67*, 5608–5613. [[CrossRef](#)] [[PubMed](#)]
14. Janissen, R.; Murillo, D.M.; Niza, B.; Sahoo, P.K.; Nobrega, M.M.; Cesar, C.L.; Temperini, M.L.A.; Carvalho, H.F.; de Souza, A.A.; Cotta, M.A. Spatiotemporal distribution of different extracellular polymeric substances and filamentation mediate *Xylella fastidiosa* adhesion and biofilm formation. *Sci. Rep.* **2015**, *5*, 9856. [[CrossRef](#)] [[PubMed](#)]
15. Kostakioti, M.; Hadjifrangiskou, M.; Hultgren, S.J. Bacterial biofilms: Development, dispersal, and therapeutic strategies in the dawn of the postantibiotic era. *Cold Spring Harb. Perspect. Med.* **2013**, *3*, a010306. [[CrossRef](#)] [[PubMed](#)]
16. Cugini, C.; Shanmugam, M.; Landge, N.; Ramasubbu, N. The role of exopolysaccharides in oral biofilms. *J. Dent. Res.* **2019**, *98*, 739–745. [[CrossRef](#)]
17. Murthy, P.S.; Venkatesan, R. Industrial biofilms and their control. In *Marine and Industrial Biofouling*; Flemming, H.C., Murthy, P.S., Venkatesan, R., Cooksey, K., Eds.; Springer Series on Biofilms; Springer: Berlin/Heidelberg, Germany, 2008; Volume 4, pp. 65–101. ISBN 978-3-540-69794-7.
18. Robert Antony, A.; Janani, R.; Rajesh Kannan, V. Biofilm instigation of plant pathogenic bacteria and its control measures. In *Biofilms in Plant and Soil Health*; John Wiley & Sons, Ltd: Chichester, UK, 2017; pp. 409–438.
19. Galié, S.; García-Gutiérrez, C.; Miguélez, E.M.; Villar, C.J.; Lombó, F. Biofilms in the food industry: Health aspects and control methods. *Front. Microbiol.* **2018**, *9*, 898. [[CrossRef](#)]
20. Sena-Velez, M.; Redondo, C.; Gell, I.; Ferragud, E.; Johnson, E.; Graham, J.H.; Cubero, J. Biofilm formation and motility of *Xanthomonas* strains with different citrus host range. *Plant Pathol.* **2015**, *64*, 767–775. [[CrossRef](#)]
21. Guerra, M.L.; Malafaia, C.B.; Macedo, A.J.; Silva, M.V.; Mariano, R.L.R.; Souza, E.B. Biofilm formation by *Xanthomonas campestris* pv. *viticola* affected by abiotic surfaces and culture media. *Trop. Plant Pathol.* **2018**, *43*, 146–151. [[CrossRef](#)]
22. Redondo, C.; Sena-Vélez, M.; Gell, I.; Ferragud, E.; Sabuquillo, P.; Graham, J.H.; Cubero, J. Influence of selected bactericides on biofilm formation and viability of *Xanthomonas citri* subsp. *citri*. *Crop Prot.* **2015**, *78*, 204–213. [[CrossRef](#)]
23. Lawrence, J.R.; Delaquis, P.J.; Korber, D.R.; Caldwell, D.E. Behavior of *Pseudomonas fluorescens* within the hydrodynamic boundary layers of surface microenvironments. *Microb. Ecol.* **1987**, *14*, 1–14. [[CrossRef](#)]
24. Sauer, K.; Camper, A.K.; Ehrlich, G.D.; Costerton, J.W.; Davies, D.G. *Pseudomonas aeruginosa* displays multiple phenotypes during development as a biofilm. *J. Bacteriol.* **2002**, *184*, 1140–1154. [[CrossRef](#)]
25. Harshey, R.M. Bacterial motility on a surface: Many ways to a common goal. *Annu. Rev. Microbiol.* **2003**, *57*, 249–273. [[CrossRef](#)] [[PubMed](#)]
26. Czaczyk, K.; Myszka, K. Biosynthesis of extracellular polymeric substances (EPS) and its role in microbial biofilm formation. *Polish J. Environ. Stud.* **2007**, *16*, 799–806.
27. Salama, Y.; Chennaoui, M.; Sylla, A.; Mountadar, M.; Rihani, M.; Assobhei, O. Characterization, structure, and function of extracellular polymeric substances (EPS) of microbial biofilm in biological wastewater treatment systems: A review. *Desalin. Water Treat.* **2016**, *57*, 16220–16237. [[CrossRef](#)]
28. Stoodley, P.; Dodds, I.; Boyle, J.D.; Lappin-Scott, H.M. Influence of hydrodynamics and nutrients on biofilm structure. *J. Appl. Microbiol. Symp. Suppl.* **1999**, *85*, 19S–28S. [[CrossRef](#)]
29. Parsek, M.R.; Tolker-Nielsen, T. Pattern formation in *Pseudomonas aeruginosa* biofilms. *Curr. Opin. Microbiol.* **2008**, *11*, 560–566. [[CrossRef](#)]
30. Harmsen, M.; Yang, L.; Pamp, S.J.; Tolker-Nielsen, T. An update on *Pseudomonas aeruginosa* biofilm formation, tolerance, and dispersal. *FEMS Immunol. Med. Microbiol.* **2010**, *59*, 253–268. [[CrossRef](#)] [[PubMed](#)]
31. Cooke, A.C.; Nello, A.V.; Ernst, R.K.; Schertzer, J.W. Analysis of *Pseudomonas aeruginosa* biofilm membrane vesicles supports multiple mechanisms of biogenesis. *PLoS ONE* **2019**, *14*, e0212275. [[CrossRef](#)] [[PubMed](#)]
32. Kulp, A.; Kuehn, M.J. Biological Functions and biogenesis of secreted bacterial outer membrane vesicles. *Annu. Rev. Microbiol.* **2010**, *64*, 163–184. [[CrossRef](#)] [[PubMed](#)]
33. Garita-Cambronero, J.; Palacio-Bielsa, A.; Cubero, J. *Xanthomonas arboricola* pv. *pruni*, causal agent of bacterial spot of stone fruits and almond: Its genomic and phenotypic characteristics in the *X. arboricola* species context. *Mol. Plant Pathol.* **2018**, *19*, 2053–2065. [[CrossRef](#)]
34. Garita-Cambronero, J.; Sena-Vélez, M.; Ferragud, E.; Sabuquillo, P.; Redondo, C.; Cubero, J. *Xanthomonas citri* subsp. *citri* and *Xanthomonas arboricola* pv. *pruni*: Comparative analysis of two pathogens producing similar symptoms in different host plants. *PLoS ONE* **2019**, *14*, e0219797. [[CrossRef](#)]
35. Martínez, L.C.; Vadyvaloo, V. Mechanisms of post-transcriptional gene regulation in bacterial biofilms. *Front. Cell. Infect. Microbiol.* **2014**, *5*, 1–15. [[CrossRef](#)]



36. Garita-Cambronero, J.; Palacio-Bielsa, A.; López, M.M.; Cubero, J. Comparative genomic and phenotypic characterization of pathogenic and non-pathogenic strains of *Xanthomonas arboricola* reveals insights into the infection process of bacterial spot disease of stone fruits. *PLoS ONE* **2016**, *11*, e0161977. [\[CrossRef\]](#)
37. Wengelnik, K.; Marie, C.; Russel, M.; Bonas, U. Expression and localization of HrpA1, a protein of *Xanthomonas campestris* pv. vesicatoria essential for pathogenicity and induction of the hypersensitive reaction. *J. Bacteriol.* **1996**, *178*, 1061–1069. [\[CrossRef\]](#)
38. O'Toole, G.A.; Pratt, L.A.; Watnick, P.I.; Newman, D.K.; Weaver, V.B.; Kolter, R. Genetic approaches to study of biofilms. *Methods Enzymol.* **1999**, *310*, 91–109.
39. Kraiselburd, I.; Alet, A.I.; Tondo, M.L.; Petrocelli, S.; Daurelio, L.D.; Monzón, J.; Ruiz, O.A.; Losi, A.; Orellano, E.G. A LOV protein modulates the physiological attributes of *Xanthomonas axonopodis* pv. citri relevant for host plant colonization. *PLoS ONE* **2012**, *7*, e38226.
40. Smirnova, T.A.; Didenko, L.V.; Azizbekyan, R.R.; Romanova, Y.M. Structural and functional characteristics of bacterial biofilms. *Microbiology* **2010**, *79*, 413–423. [\[CrossRef\]](#)
41. Lu, X.H.; An, S.Q.; Tang, D.J.; McCarthy, Y.; Tang, J.L.; Dow, J.M.; Ryan, R.P. RsmA regulates biofilm formation in *Xanthomonas campestris* through a regulatory network involving cyclic di-GMP and the Clp transcription factor. *PLoS ONE* **2012**, *7*, e52646. [\[CrossRef\]](#)
42. Ficarra, F.A.; Grandellis, C.; Galván, E.M.; Ielpi, L.; Feil, R.; Lunn, J.E.; Gottig, N.; Ottado, J. *Xanthomonas citri* ssp. *citri* requires the outer membrane porin OprB for maximal virulence and biofilm formation. *Mol. Plant Pathol.* **2017**, *18*, 720–733. [\[CrossRef\]](#)
43. Sahu, S.K.; Zheng, P.; Yao, N. Niclosamide blocks rice leaf blight by inhibiting biofilm formation of *Xanthomonas oryzae*. *Front. Plant Sci.* **2018**, *9*, 1–16. [\[CrossRef\]](#)
44. Park, H.; Do, E.; Kim, M.; Park, H.J.; Lee, J.; Han, S.W. A LysR-Type Transcriptional Regulator LcrX Is Involved in virulence, biofilm formation, swimming motility, siderophore secretion, and growth in sugar sources in *Xanthomonas axonopodis* pv. *glycines*. *Front. Plant Sci.* **2020**, *10*, 1657. [\[CrossRef\]](#)
45. Karatan, E.; Watnick, P. Signals, regulatory networks, and materials That build and break bacterial biofilms. *Microbiol. Mol. Biol. Rev.* **2009**, *73*, 310–347. [\[CrossRef\]](#)
46. Absalon, C.; van Dellen, K.; Watnick, P.I. A communal bacterial adhesin anchors biofilm and bystander cells to surfaces. *PLoS Pathog.* **2011**, *7*, e1002210. [\[CrossRef\]](#)
47. Kjelleberg, S.; Hermansson, M. Starvation-induced effects on bacterial surface characteristics. *Appl. Environ. Microbiol.* **1984**, *48*, 497–503. [\[CrossRef\]](#)
48. Simões, M.; Simões, L.C.; Vieira, M.J. A review of current and emergent biofilm control strategies. *LWT Food Sci. Technol.* **2010**, *43*, 573–583. [\[CrossRef\]](#)
49. Donlan, R.M.; Costerton, J.W. Biofilms: Survival mechanisms of clinically relevant microorganisms. *Clin. Microbiol. Rev.* **2002**, *15*, 167–193. [\[CrossRef\]](#)
50. Wai, S.N.; Mizunoe, Y.; Takade, A.; Kawabata, S.I.; Yoshida, S.I. *Vibrio cholerae* O1 strain TSI-4 produces the exopolysaccharide materials that determine colony morphology, stress resistance, and biofilm formation. *Appl. Environ. Microbiol.* **1998**, *64*, 3648–3655. [\[CrossRef\]](#)
51. Hoa, P.T.; Nair, L.; Visvanathan, C. The effect of nutrients on extracellular polymeric substance production and its influence on sludge properties. *Water* **2003**, *29*, 437–442. [\[CrossRef\]](#)
52. Sanchez, Z.; Tani, A.; Suzuki, N.; Kariyama, R.; Kumon, H.; Kimbara, K. Assessment of change in biofilm architecture by nutrient concentration using a multichannel microdevice flow system. *J. Biosci. Bioeng.* **2013**, *115*, 326–331. [\[CrossRef\]](#) [\[PubMed\]](#)
53. Lorite, G.S.; Janissen, R.; Clerici, J.H.; Rodrigues, C.M.; Tomaz, J.P.; Mizaikoff, B.; Kranz, C.; de Souza, A.A.; Cotta, M.A. Surface physicochemical properties at the micro and nano length scales: Role on bacterial adhesion and *Xylella fastidiosa* biofilm development. *PLoS ONE* **2013**, *8*, e75247.
54. Kreft, J.U. Biofilms promote altruism. *Microbiology* **2004**, *150*, 2751–2760. [\[CrossRef\]](#) [\[PubMed\]](#)
55. Karlyshev, A.V.; McCrossan, M.V.; Wren, B.W. Demonstration of polysaccharide capsule in *Campylobacter jejuni* using electron microscopy. *Infect. Immun.* **2001**, *69*, 5921–5924. [\[CrossRef\]](#)
56. Dawson, M.P.; Humphrey, B.A.; Marshall, K.C. Adhesion: A tactic in the survival strategy of a marine vibrio during starvation. *Curr. Microbiol.* **1981**, *6*, 195–198. [\[CrossRef\]](#)
57. Espinal, P.; Martí, S.; Vila, J. Effect of biofilm formation on the survival of *Acinetobacter baumannii* on dry surfaces. *J. Hosp. Infect.* **2012**, *80*, 56–60. [\[CrossRef\]](#)
58. Serra, D.O.; Richter, A.M.; Klauck, G.; Mika, F.; Hengge, R. Microanatomy at cellular resolution and spatial order of physiological differentiation in a bacterial biofilm. *MBio* **2013**, *4*, e00103. [\[CrossRef\]](#)
59. Van Gerven, N.; Van der Verren, S.E.; Reiter, D.M.; Remaut, H. The Role of functional amyloids in bacterial virulence. *J. Mol. Biol.* **2018**, *430*, 3657–3684. [\[CrossRef\]](#)
60. Barnhart, M.M.; Chapman, M.R. Curli biogenesis and function. *Annu. Rev. Microbiol.* **2006**, *60*, 131–147. [\[CrossRef\]](#)
61. Rigano, L.A.; Siciliano, F.; Enrique, R.; Sendín, L.; Filippone, P.; Torres, P.S.; Qüesta, J.; Dow, J.M.; Castagnaro, A.P.; Vojnov, A.A.; et al. Biofilm formation, epiphytic fitness, and canker development in *Xanthomonas axonopodis* pv. *citri*. *Mol. Plant-Microbe Interact.* **2007**, *20*, 1222–1230. [\[CrossRef\]](#)
62. Davey, M.E.; Caiazza, N.C.; O'Toole, G.A. Rhamnolipid surfactant production affects biofilm architecture in *Pseudomonas aeruginosa* PAO1. *J. Bacteriol.* **2003**, *185*, 1027–1036. [\[CrossRef\]](#) [\[PubMed\]](#)

63. Lawrence, J.R.; Caldwell, D.E. Behavior of bacterial stream populations within the hydrodynamic boundary layers of surface microenvironments. *Microb. Ecol.* **1987**, *14*, 15–27. [[CrossRef](#)]
64. Webb, J.S.; Thompson, L.S.; James, S.; Charlton, T.; Tolker-Nielsen, T.; Koch, B.; Givskov, M.; Kjelleberg, S. Cell death in *Pseudomonas aeruginosa* biofilm development. *J. Bacteriol.* **2003**, *185*, 4585–4592. [[CrossRef](#)]
65. Lee, H.H.; Molla, M.N.; Cantor, C.R.; Collins, J.J. Bacterial charity work leads to population-wide resistance. *Nature* **2010**, *467*, 82–85. [[CrossRef](#)] [[PubMed](#)]
66. Zemke, A.C.; Bomberger, J.M. Microbiology: Social suicide for a good cause. *Curr. Biol.* **2016**, *26*, 80–82. [[CrossRef](#)] [[PubMed](#)]
67. Turnbull, L.; Toyofuku, M.; Hynen, A.L.; Kurosawa, M.; Pessi, G.; Petty, N.K.; Osvath, S.R.; Cárcamo-Oyarce, G.; Gloag, E.S.; Shimoni, R.; et al. Explosive cell lysis as a mechanism for the biogenesis of bacterial membrane vesicles and biofilms. *Nat. Commun.* **2016**, *7*, 11220. [[CrossRef](#)] [[PubMed](#)]
68. Loessner, M.J.; Maier, S.K.; Daubek-Puza, H.; Wendlinger, G.; Scherer, S. Three *Bacillus cereus* bacteriophage endolysins are unrelated but reveal high homology to cell wall hydrolases from different bacilli. *J. Bacteriol.* **1997**, *179*, 2845–2851. [[CrossRef](#)] [[PubMed](#)]
69. Civerolo, E.L. Relationships of *Xanthomonas pruni* bacteriophages to bacterial spot disease in *Prunus*. *Phytopathology* **1973**, *63*, 1279. [[CrossRef](#)]
70. Zaccardelli, M.; Saccardi, A.; Gambin, E.; Mazzuchi, U. *Xanthomonas campestris* pv. *pruni* bacteriophages on peach trees and their potential use for biological control. *Phytopathol. Mediterr.* **1992**, *31*, 133–140.
71. Gill, S.; Catchpole, R.; Forterre, P. Extracellular membrane vesicles in the three domains of life and beyond. *FEMS Microbiol. Rev.* **2019**, *43*, 273–303. [[CrossRef](#)]
72. Schooling, S.R.; Beveridge, T.J. Membrane vesicles: An overlooked component of the matrices of biofilms. *J. Bacteriol.* **2006**, *188*, 5945–5957. [[CrossRef](#)]
73. Singorenko, P.D.; Chang, V.; Whitcombe, A.; Simonov, D.; Hong, J.; Phillips, A.; Swift, S.; Blenkiron, C. Isolation of membrane vesicles from prokaryotes: A technical and biological comparison reveals heterogeneity. *J. Extracell. Vesicles* **2017**, *6*, 1324731. [[CrossRef](#)]
74. Rybak, K.; Robatzek, S. Functions of extracellular vesicles in immunity and virulence. *Plant Physiol.* **2019**, *179*, 1236–1247. [[CrossRef](#)] [[PubMed](#)]
75. Biller, S.J.; Schubotz, F.; Roggensack, S.E.; Thompson, A.W.; Summons, R.E.; Chisholm, S.W. Bacterial vesicles in marine ecosystems. *Science* **2014**, *343*, 183–186. [[CrossRef](#)] [[PubMed](#)]